

pubs.acs.org/NanoLett Letter

Dielectric Engineering for Manipulating Exciton Transport in Semiconductor Monolayers

Zidong Li, Darwin F. Cordovilla Leon, Woncheol Lee, Kanak Datta, Zhengyang Lyu, Jize Hou, Takashi Taniguchi, Kenji Watanabe, Emmanouil Kioupakis, and Parag B. Deotare*



Cite This: https://doi.org/10.1021/acs.nanolett.1c02990



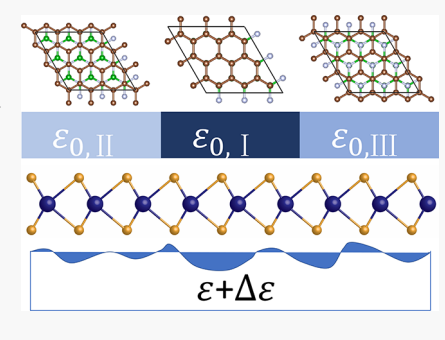
ACCESS

Metrics & More

Article Recommendations

s Supporting Information

ABSTRACT: The dielectric screening from the disordered media surrounding atomically thin transition metal dichalcogenides (TMDs) monolayers modifies the effective defect energy levels and thereby the transport and energy dynamics of excitons. In this work, we study this effect in WSe₂ monolayers for different combinations of surrounding dielectric media. Specifically, we study the source of the anomalous diffusion of excitons in the WSe₂ monolayer and attribute the anomaly to the modification of the energy distribution of defect states in different disordered dielectric environments. We use this insight to manipulate exciton transport by engineering the dielectric environment using a graphene/hexagonal boron nitride (h-BN) moiré superlattice. Finally, we observe that the effect of dielectric disorder is even more significant at high excitation fluences, contributing to the nonequilibrium phonon drag effect. These results provide an



important step toward achieving control over the exciton energy transport for next-generation opto-excitonic devices.

KEYWORDS: dielectric environment, exciton transport, moiré superlattice, transition metal dichalcogenides

INTRODUCTION

The transport of excitons in two-dimensional (2D) semi-conductors such as transition metal dichalcogenides (TMDs) monolayers and van der Waals heterostructures is significantly affected by the surrounding since the electric field lines that bind the exciton extends far outside the 2D materials. Thus, any fluctuations due to the nonuniform dielectric surroundings, interfacial charges and impurities as well as substrate phonons inhibit the transport of excitons in TMD monolayers. In addition, exciton transport is significantly restricted by intrinsic structural defects such as vacancies, grain boundaries and antistites. The influence of defects, however, can be mitigated by carefully engineering the dielectric surroundings by isolating the monolayers from defects that contribute to the energetic disorder experienced by excitons.

In this work, we directly monitor the diffusion of excitons in WSe₂ monolayers experiencing different disordered dielectric surroundings via temporally and spatially resolved photoluminescence (PL) imaging at room temperature. Specifically, we report the effect of the disordered dielectric surroundings on the distribution of defect states (inferred from PL) and correlate it with the observed anomalous diffusion (time varying diffusivity) of excitons at low excitation densities and the phonon drag effect^{12–14} at high excitation densities. These results confirm that h-BN encapsulation considerably improves the transport performance of excitons and reduces their Auger recombination rate relative to excitons in bare WSe₂ on SiO₂/Si substrates in agreement with other reports. We attribute such an enhancement in the transport of excitons to the

reduced dielectric disorder, which modifies the energy distribution of defect states. With the developed understanding, we manipulate transport by creating a controlled dielectric perturbation using a graphene/h-BN moiré superlattice. We further confirm the findings by investigating transport at high exciton densities and find that the halo formation observed in the exciton density distribution is directly related to the defect distribution. The findings support that the phonon drag ^{12,14,16} initiated by the trap-assisted Auger process leads to halo formation as opposed to electron—hole liquid. ^{17,18}

■ RESULTS AND DISCUSSION

We studied the influence of the surrounding dielectric media on the exciton PL, absorption, and transport by preparing monolayer WSe₂ samples using three commonly used transfer techniques (see the "Methods" section and Supporting Information section 1): direct exfoliation on a SiO₂/Si substrate, PDMS-assisted transfer¹⁹ on a SiO₂/Si substrate, and h-BN encapsulation. Excitons in samples prepared using direct exfoliation (Sample I) were the least screened: a bare monolayer WSe₂ transferred on top of a SiO₂/Si substrate ($\varepsilon_{\rm t}$ =

Received: August 3, 2021 Revised: September 22, 2021



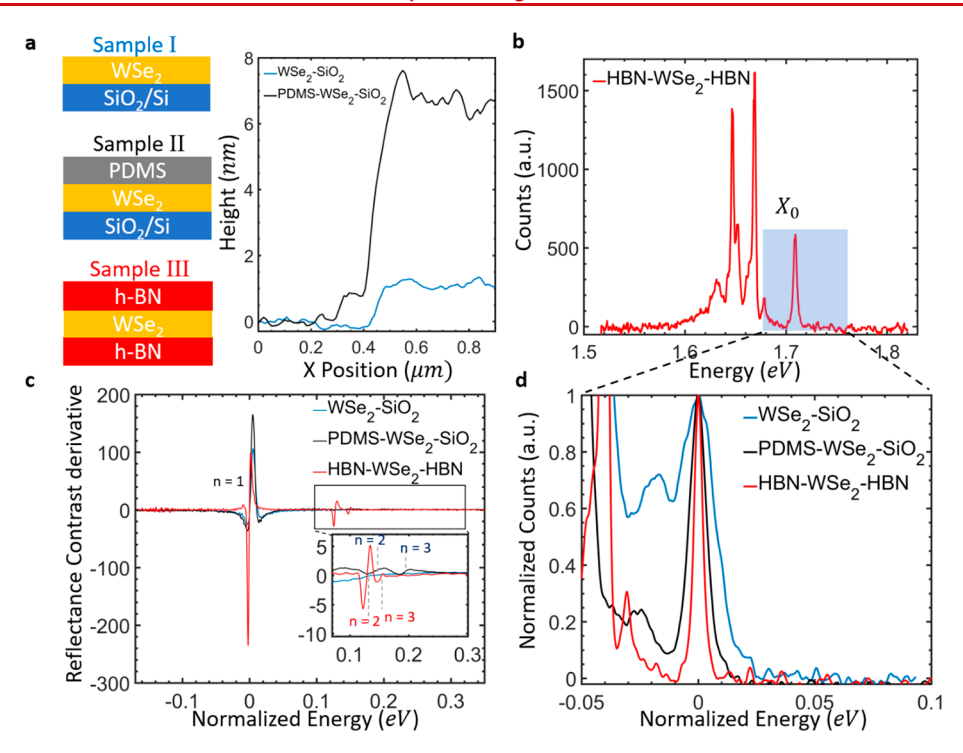


Figure 1. Excitons in different disordered dielectric environments. (a) Schematic showing a WSe₂ monolayer prepared using three transfer techniques that result in different dielectric surrounding environments. AFM scans confirm a 5–6 nm thick residual PDMS layer for PDMS-assisted transfer. (b) PL spectrum of the h-BN encapsulated monolayer WSe₂ at 4.2 K. (c) Low-temperature first derivative of the reflectance contrast of bare monolayer WSe₂ on SiO₂ substrate (blue), monolayer WSe₂ with a thin PDMS top layer on SiO₂ substrate (black), and h-BN encapsulated monolayer WSe₂ (red). The inset shows a zoomed region of the first excited state (n = 2) and the second excited state (n = 3). The x-axis of the spectrum is normalized with respect to the ground-state exciton energy. (d) Comparison of the exciton PL line width at 4.2 K between the bare monolayer WSe₂ on SiO₂ substrate (blue), the monolayer WSe₂ with a thin PDMS top layer on SiO₂ substrate (black), and the h-BN encapsulated monolayer WSe₂ (red). The x-axis of the PL spectrum is normalized to the neutral exciton energy.

1, $\varepsilon_{\rm b}=2.1$), where $\varepsilon_{\rm t}$ and $\varepsilon_{\rm b}$ represents the top and the bottom relative dielectric permittivity, respectively. Excitons in sample II experienced relatively more screening than excitons in sample I due to a thin residual layer (5–6 nm) of PDMS ($\varepsilon_{\rm t}=2.4$) on top of the monolayer (confirmed using atomic force microscope (AFM), Figures 1a and S2). Excitons in the h-BN (thickness ~30 nm) encapsulated monolayer WSe₂ (Sample III) experienced the most screening due to the higher dielectric permittivity ($\varepsilon_{\rm b}=\varepsilon_{\rm t}=4.5$) of the surrounding. We note that the dielectric constants mentioned here correspond to the high-frequency values.²⁰

Figure 1b shows the low-temperature PL spectrum of the h-BN encapsulated sample at low excitation fluence (22.7 nJ/ cm², 3.1 eV pulsed laser). This prevents formation of higherorder correlated excitonic states (biexcitons, charged biexcitons, etc.). 21-23 We were able to identify well resolved peaks corresponding to excitons, trions, neutral and charged dark excitons and various phonon replicas as reported in literature. 24-27 However, such peaks could not be resolved in samples I and II because of the large inhomogeneous broadening (see Figure S3). The line width of the neutral excitons (shaded region in Figure 1b) was extracted to be 16.08 ± 0.42 meV, 9.68 ± 0.15 meV, and 4.27 ± 0.06 meV (see Figure 1d) for samples I-III, respectively. The WSe₂ monolayers for all the samples were exfoliated from the same bulk crystal; therefore, we expect similar intrinsic defect (vacancy/substitutional) density in all samples. We assume that the homogeneous broadening due to exciton-phonon scattering was comparable at 4.2 K (quantitative comparison requires further theoretical development). We also expect contribution to homogeneous broadening from exciton-exciton scattering to be negligible due to the low exciton density (\sim 4.6 \times 10¹⁰/cm²). Hence, we attribute the difference in the exciton PL line width to the disorder in the dielectric surroundings, defined as the local variations of the external dielectric permittivity ($\Delta\varepsilon_{\rm ext}$). The dielectric disorder, caused by surface roughness, impurities, adsorbates, vacancies, and dangling bonds from the substrates, modifies the excitonic energy, resulting in an inhomogeneous broadening of the exciton PL line width.

The locally varying surrounding permittivity modulates the excitonic resonances. However, the modulation of the exciton ground state resonance (n = 1) due to the varying surrounding dielectric is relatively small. 20,29 This is because the resulting bandgap renormalization, is nearly compensated by the change in exciton binding energy. ^{30,31} On the other hand, the energies of the excited states $(n \ge 2)$ strongly depend on the surrounding dielectrics and thus, the inhomogeneous broadening is more susceptible to the dielectric disorder. Figure 1c plots the derivative of the low-temperature reflectance contrast of the three samples. The inset shows that the line width of the first excited-state resonances(n = 2) increases from 6.7 meV for the h-BN encapsulated WSe₂ (red) to 25.8 meV for the PDMS-WSe₂ on SiO₂ (black). For the bare WSe₂ on SiO₂ (blue), the broad excited-state resonances are barely resolvable. The low-temperature PL and reflection measurements indicate the following dielectric order relationship: $\Delta \varepsilon_{\text{ext-bare}} > \Delta \varepsilon_{\text{ext-PDMS}} > \Delta \varepsilon_{\text{ext-hBN}}$. Excitons in the bare WSe₂ on SiO₂ are susceptible to the dielectric fluctuations from both the substrate as well as adsorbates from air (adsorbed during

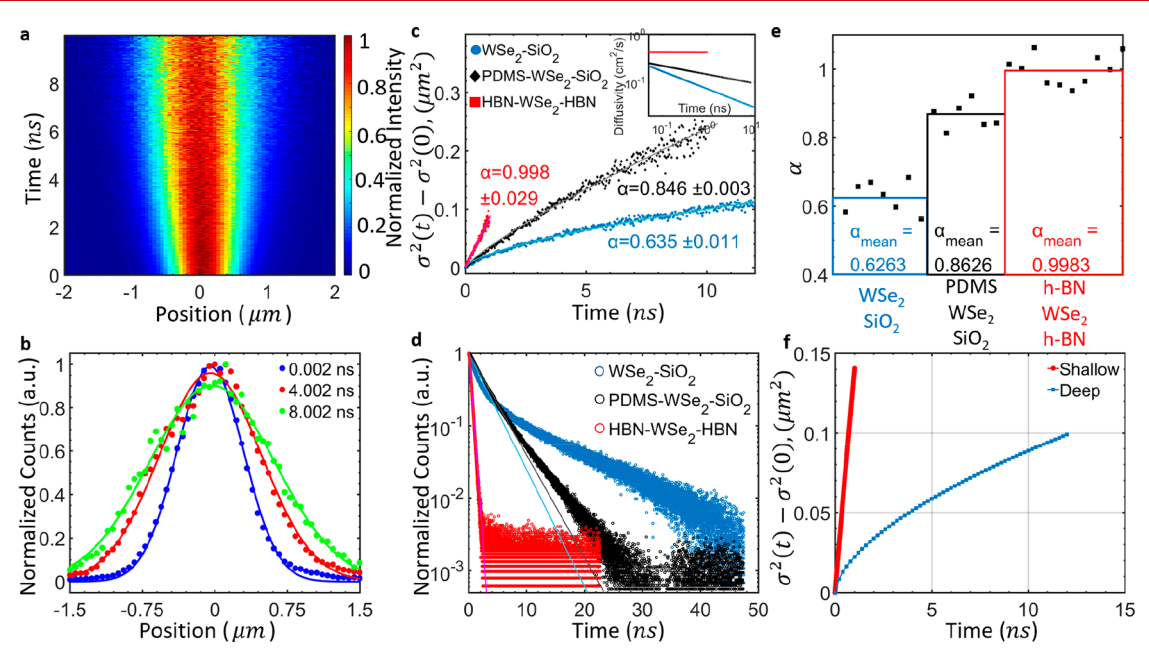


Figure 2. Exciton diffusion and dynamics in a disordered dielectric environment. (a) Normalized exciton density as a function of position and time obtained with an avalanche photodiode detector (APD) and time-correlated single photon counting (TCSPC). (b) Time slices of the normalized exciton density distribution fitted with Gaussians showing the broadening of the exciton distribution. (a, b) are from the PDMS transferred sample that has a thin layer of PDMS on top of the monolayer WSe₂. (c) Evolution of the change in mean squared displacement (MSD) of the exciton density distribution in bare WSe₂ on SiO₂/Si substrate (blue dots), PDMS-WSe₂ on SiO₂/Si substrate (black diamonds) and h-BN encapsulated WSe₂ (red squares). The time window used to display each curve corresponds to the time when the photoluminescence (PL) intensity dropped to 5% of its initial value. The solid lines are fits using eq 1. The inset shows the time-dependent diffusivities for the three samples. (d) Room-temperature time-resolved Photoluminescence (TRPL) intensity of excitons in bare WSe₂ on SiO₂/Si substrate (blue), PDMS-WSe₂ on SiO₂/Si substrate (black), and h-BN encapsulated WSe₂ (red). The solid lines are single exponential fits. (e) Summary of the anomalous exciton diffusion coefficients from different samples prepared by different methods. (f) Calculated evolution of the change of MSD in the presence of an exponential distribution of trap states using the multitrapping limited exciton transport model.

exfoliation).^{32–34} Covering the top with a thin layer of PDMS reduces the dielectric fluctuation from air without altering the substrate induced dielectric disorder. Encapsulation with high-quality h-BN flakes provides the best dielectric surroundings with negligible dielectric fluctuations.

The dielectric disorder also alters the distribution of intrinsic defect states. However, it is difficult to study the effect in monolayer WSe₂, since the low-temperature PL spectrum is quite complex due to the existence of various dark and phonon sidebands states. The identification of the defect level thus remains contentious.^{35–37} Therefore, to study the impact of dielectric disorder on the defect distributions in monolayer TMDs, we use the well-studied monolayer molybdenum disulfide (MoS₂) shown in the Figure S4. We identified two charged defect-bound excitons (XD1, XD2) at the sulfur vacancies^{32,38-41} peak at ~150 and ~400 meV below the neutral exciton X⁰, respectively. Both peaks show a heavy tail at lower energy. In agreement with the reported first-principles calculations, 2,42 the effective charged defect levels (see arrows in Figure S4) in MoS2 experience a deep to shallow transition as the screening by the dielectric environment increases. Along with the shift in peak energy, the deep-tailed energy distribution also shrinks with decreasing dielectric disorders. Thus, the effective intrinsic defect depth is altered by the surrounding dielectric. We expect similar effect for monolayer ${
m WSe}_2$ that leads to the following defect depth trend: $U_{
m h\text{-}BNencap}$ $< U_{
m PDMS} < U_{
m bare}$. Such defects act as traps and barriers that impede the diffusion and the recombination dynamics of excitons at room temperature.

We confirm the hypothesis by monitoring the transport (directly affected by the dielectric disorder) of excitons by imaging the time-dependent change in exciton spatial distribution as shown in Figure 2a,b, using the scanningtime-correlated single-photon counting technique outlined in our previous work. 43,44 The laser excitation fluence was set low (22.7 nJ/cm²) to minimize the nonequilibrium many-body effects.²⁸ (PL intensity at a certain time and space is proportional to the exciton density at the same time and space; see Figures S6 and S7.) When a low density (4.6 × 10¹⁰/cm²) of excitons is in thermal equilibrium with the lattice (see Figure S8), the transport of the excitons is limited by their interactions with phonons and defects (both elastic and inelastic scattering can affect the diffusivity/mobility). Under such conditions, the change of mean squared displacement (MSD) of a Gaussian spatial distribution of excitons denoted by $\Delta \sigma^2(t)$ evolves linearly with time according to $\Delta \sigma^2(t) \equiv$ $\sigma^2(t) - \sigma^2(0) = 2Dt$, where $2\sigma(t)$ represents the width of the Gaussian exciton distribution at time t, and D is the free exciton diffusion coefficient or diffusivity. However, energetic disorder due to crystal (intrinsic) and substrate (extrinsic) induced defects lead to exciton trapping. In such a case, the change in MSD no longer evolves linearly with time, resulting in a time-varying diffusion coefficient. Under such circumstances, the nonlinear evolution of the change of MSD (referred as anomalous diffusion) is typically described by the power-law model⁴⁴

$$\Delta \sigma^2(t) = \Phi t^{\alpha} \tag{1}$$

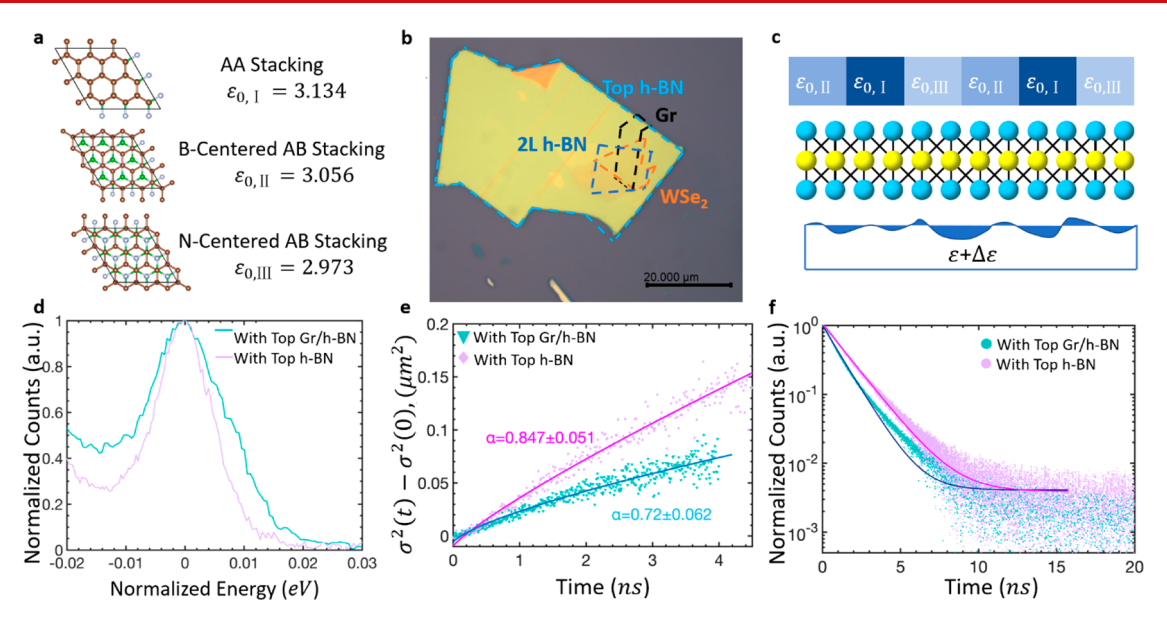


Figure 3. Engineering dielectric disorder. (a) Illustration of different stackings from the h-BN/Graphene moiré superlattice. The microscopic dielectric constant of each stacking configuration ($\varepsilon_{0,l}$, $\varepsilon_{0,ll}$ and $\varepsilon_{0,lll}$) is obtained from first-principles calculations. (b) Bright-field optical image of a top h-BN/graphene/bilayer h-BN/WSe₂ heterostructure on a SiO₂/Si substrate. (c) Schematic of a monolayer WSe₂ sandwiched between an engineered dielectric environment (h-BN/Graphene moiré superlattice) and a randomly disordered dielectric environment (SiO₂/Si substrate). (d) Comparison of the exciton PL line width at 4.2 K with and without the Graphene layer. (e) Evolution of the change of MSD of the exciton density distribution in the WSe₂ monolayer with (azure triangles) and without (purple dots) the graphene layer. The time window used to display each curve corresponds to the time when the TRPL intensity dropped to 5% of its peak value. The solid lines are fits using eq 1. (f) TRPL intensity of excitons in the WSe₂ monolayer with (azure dots) and without (purple dots) the graphene layer. The solid lines are fits using single-exponential decay with a constant offset.

where Φ and α denote the transport factor and anomalous coefficient, respectively. In the case when $\alpha=1$, the evolution reverts to normal Fick's law of diffusion, and the diffusion coefficient ($D=\Phi/2$) remains constant with time. The anomalous coefficient thus describes the degree of nonlinearity for the change of MSD.

Figure 2c plots the evolution of the change of MSD for different samples. The time windows were fixed to a value corresponding to a drop in TRPL intensity to 5% of its initial value. We observed that excitons in WSe₂ encapsulated by h-BN undergo normal diffusion (α = 0.998 ± 0.029). In contrast, the excitons in bare WSe₂ on SiO₂ and PDMS-WSe₂ on SiO₂ evolved nonlinearly (α = 0.635 ± 0.011 and α = 0.846 ± 0.003, respectively). Multiple samples were examined to verify the repeatability of this observation as shown in Figure 2e. The sublinear expansion of the change of MSD points to a time-dependent effective diffusivity (Figure 2c inset), defined as

$$D'(t) \equiv \left(\frac{1}{2}\right) \left(\frac{\partial \Delta \sigma^{2}(t)}{\partial t}\right) = \left(\frac{\alpha \Phi t^{\alpha - 1}}{2}\right) \tag{2}$$

Such differences in the observed anomalous coefficient and the effective diffusivities across the different samples can be explained by a multitrapping and release (MTR) exciton transport model⁴⁵ shown in Figure 2f. In energetically disordered semiconductors under the low excitation density limit, transport becomes sub-diffusive due to the capture (temporary or until recombined) of mobile excitons at trap sites. The amount of time an exciton remains trapped depends on the energy distribution of trap states. If the energy distribution of traps is non-Gaussian or has a nonvanishing deep-level "tail", as suggested by the low temperature PL (see Figures S4 and S5), then the excitons remain localized for extended period (relative to the recombination time). The

transport of the excitons slows down due to the multiple trap and escape events resulting in nonlinear evolution of the change of MSD. In the limit of high energetic disorder defined as the limit where the excitons spend more time being trapped than moving freely in the band, the effective diffusivity of excitons experiencing a deep-tailed exponential energy distribution of traps can be represented as (see Support Information notes 7),

$$D'(t) = \eta(t) D \approx \frac{D}{\Gamma(\alpha)} \left(\frac{t}{\theta}\right)^{\alpha-1}$$
 (3)

where $\eta(t) = n_{\rm f}(t)/[n_{\rm f}(t) + n_{\rm f}(t)]$ is the fraction of mobile or delocalized excitons from the total population comprising of free $n_{\rm f}(t)$ and trapped excitons $n_{\rm t}(t)$, and D is the scatteringlimited, free-exciton diffusivity, $\Gamma(\alpha)$ is the gamma function, the parameter θ controls the dynamics of trapping as it depends on both the capture and escape rates, $\alpha \equiv \frac{k_B T}{U}$ is the anomalous coefficient, and U_t is the effective trap depth, which is inversely proportional to the anomalous coefficient. Therefore, the effective trap depth can be extracted from the nonlinearity of the change of MSD as $U_{\text{h-BNencap}} < U_{\text{PDMS}} <$ U_{bare} . Figure 2f shows the calculated evolution of the change of MSD based on the multitrapping and release model for a trapping environment with deep (blue squares)/shallow (red circles) traps. All other parameters were same for both calculations. The results are consistent with the experimental results shown in Figure 2c.

A similar conclusion can be drawn by examining the TRPL. The distinct exciton lifetimes can be attributed to the varying amount of screening from the dielectric environment, hereby altering the exciton binding energy as well as the Bohr's radius. An increase in the Bohr's radius implies an increase in the

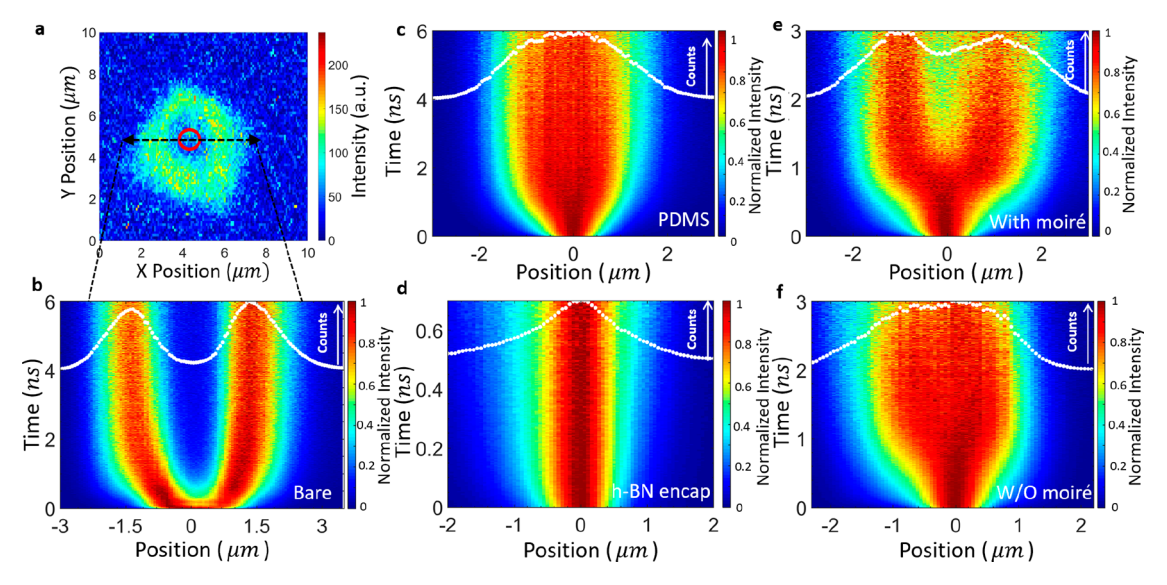


Figure 4. Exciton propagation in the phonon drag regime (18.2 μ J/cm²). (a) PL image from the bare WSe₂ monolayer on SiO₂/Si substrate showing the halo effect. The red circle indicates the laser excitation spot. (b-f) Normalized exciton density as a function of position and time for the bare WSe₂ (b), PDMS-WSe₂ (c), h-BN encapsulated WSe₂ (d), and WSe₂ with/without (e, f) the h-BN/Gr moiré superlattice. The white dots represent the spatial PL profile obtained by integrating the density distribution for the later $^{1}/_{3}$ time window.

exciton's transition dipole moment which in turn increases the rate of spontaneous emission. Apart from the significant difference between the overall exciton recombination rate, the decaying behaviors of the TRPL of excitons in different dielectric surroundings reveals the impact of defects on exciton recombination as shown in Figure 2d. Since we kept the incident laser fluence at an extremely low level, the nonequilibrium many-body effects such as Auger recombination can be neglected. Therefore, excitons in a defect-free environment decay exponentially, regardless of the binding energy/Bohr's radius. We observed such a monoexponential decay of the TRPL in sample III (h-BN encapsulated WSe2 monolayer). However, excitons in sample I (bare WSe₂ monolayer on SiO₂) show a large deviation from monoexponential decay (two recombination time scales), which is consistent with influence from long-lived, deep-level defect states. 46-48 Both, the fast and slow time constants of the biexponential decay of the TRPL intensity depend nontrivially on the recombination rates from the excitonic and defect states to the ground state as well as on the scattering rates between the defect and excitonic state. Consistently, sample II (PDMS-WSe₂ monolayer on SiO₂) shows a small deviation (shown in Figure 2d, solid fits) from the monoexponential decay of the TRPL due to a relatively shallower defect depth distribution. Such observations suggest the following trend in the effective defect depths: $U_{\text{h-BNencap}} < U_{\text{PDMS}} < U_{\text{bare}}$, in agreement with the trend portrayed from the low-temperature PL and transport measurements.

These results bring up the intriguing possibility of manipulating the transport and recombination dynamics by engineering the dielectric disorder of the surrounding media. We demonstrate this by utilizing a moiré superlattice formed by stacking graphene on h-BN to create a two-dimensional spatially periodic dielectric perturbation. For a typical moiré supercell, we estimated the dielectric constant of the AA, B-centered AB, and N-centered AB stacking location from first-principles calculations (see Support Information note 8) as shown in Figure 3a. Our calculation indicates that different stacking configurations between graphene and boron nitride

lead to different dielectric screening. This is consistent with previous reports, which predicted a variation of electronic properties for different stacking geometries of graphene-boron nitride heterostructures. 50,51 As shown in Figure 3b, we fabricated a top h-BN/graphene (Gr)/bilayer h-BN spacer/ monolayer WSe₂ heterostructure on SiO₂. The existence of the dielectric perturbation was confirmed by the creation of moiré bands in the WSe₂ monolayer resulting in the moiré replica⁵² (see Figures S10 and S11). The insertion of the bilayer h-BN spacer does not change the dielectric surrounding significantly,⁵² but it was important to reduce the charge-transfer from the monolayer WSe2 to graphene. Under such a configuration, the monolayer WSe2 was screened by a perturbed dielectric medium from the top and a randomly fluctuating dielectric medium at the bottom as illustrated in Figure 3c. Thus, the monolayer under the h-BN/Gr moiré superlattice experienced larger dielectric disorder when compared to the area of the same flake without overlying Gr. We confirmed this by the broadened neutral exciton line width at the h-BN/Gr region as shown in Figure 3d. Figure 3e shows the change of MSD of the exciton distribution measured from the region with (azure dots) and without (purple dots) the Gr at an incident laser fluence of 22.7 nJ/cm². Consistent with the earlier observations, the anomalous diffusion coefficient lphaincreased from 0.72 ± 0.062 (with top h-BN/Gr) to $0.847 \pm$ 0.051 (with top h-BN). This was further confirmed by the observed deviation of the TRPL from a monoexponential decay trend as shown in Figure 3f.

The effect of dielectric disorder on exciton transport is even more critical at elevated incident laser fluence (18.2 μ J/cm²) due to dominance of nonequilibrium many-body effects. ^{15,28} Consistent with the reported results and calculations, ^{12,14,15} we observed a long-lived halolike spatial distribution of excitons (Figure 4a,b) in sample I (bare WSe₂ monolayer on the SiO₂/Si substrate). There are two reported explanations for such phenomenon. The first is attributed to a spatial gradient in excitonic temperature, formed by strong exciton Auger recombination, which drags excitons away from the center. ^{12,13} The second is due to formation of electron—hole liquid that

suppresses the photon absorption within the electron-hole liquid region¹⁸ or due to an outward delocalization of the highly mobile electron-hole liquid.¹⁷ In our experiments, we did not observe the halo formation in samples II and III (at the same laser fluence). The PDMS-WSe₂ monolayer (sample II) showed a flat-topped Gaussian-like spatial distribution of excitons (see Figure 4c), resulting from a small amount of exciton Auger recombination.⁵³ The h-BN encapsulated monolayer WSe2 (sample III) retained the initial Gaussian shape (see Figure 4d), implying a much smaller exciton Auger recombination rate. Thus, based on the halo formation, we can infer the Auger recombination rate γ as $\gamma_{\text{h-BNencap}} < \gamma_{\text{PDMS}} \ll$ $\gamma_{\rm bare}$. We note that such a huge variance in the Auger recombination rate cannot be explained by the change of the Coulomb-mediated Auger scattering. Thus, we infer that the decisive factor is the change of the defect-assisted Auger recombination rate due to various dielectric disorders. In a defective system, the exciton detrapping rate decreases (ratio of excitons being trapped increases) with increased trap depth. 48,55,56 The portion of excitons being trapped is also proportional to the density of traps. As a result, the defectassisted Auger recombination rate increases with increasing trap depth and density. Therefore, we infer a similar trend of dielectric disorder modified effective trap depth: $U_{\text{h-BNencap}}$ < $U_{\rm PDMS} < U_{\rm bare}$.

Consistently, we observed halo formation only in the region with Gr (Figure 4 e,f), indicating that excitons under the h-BN/Gr dielectric experienced a larger Auger recombination rate due to denser and deeper traps arising from the extra dielectric modulation from the h-BN/Gr moiré superlattice. Due to the charge transfer effect from the monolayer WSe₂ to Gr, the incident laser fluence was raised to $31.9~\mu J/cm^2$ (see Figure S13 for the diffusion map at $18.2~\mu J/cm^2$) so that the exciton density was similar to the exciton density in the area without Gr at $18.2~\mu J/cm^2$. These results indicate that the halo formation in the exciton density distribution reported in literature is indeed due to phonon drag initiated by the trapassisted Auger process as opposed to electron—hole liquid.

■ CONCLUSION

In conclusion, we experimentally quantified the exciton transport in WSe2 monolayers surrounded by varying degrees of dielectric disorder. We showed that the dielectric disorder can alter the energy distribution of trap states, thereby modifying the exciton transport. The resulting anomalous diffusion under increased disorder can be reasonably explained by the multiple trapping and release exciton-transport model describing the temporary capture of mobile excitons at trap sites. The results at high densities confirm the direct correlation between the nonequilibrium phonon drag effect resulting from increased trap assisted Auger recombination rates with the halo formation in spatial exciton distribution. Furthermore, we demonstrated the capability of engineering the dielectric perturbations using a h-BN/graphene moiré superlattice to achieve control over exciton transport. These results provide an alternate route for understanding and manipulating exciton transport. Further studies investigating the relationship of exciton dynamics with controlled dielectric contrast and spatial frequency of the dielectric disorder will lead to comprehensive understanding of exciton transport in 2D materials. The improved control over the transport dynamics is critical for the design of next generation optoexcitonic devices^{57–59} for applications in energy conversion, sensing, and data communication to beyond CMOS devices.

METHODS

Sample Fabrication. Monolayers of WSe₂ and MoS₂ were prepared via mechanical exfoliation from bulk WSe₂ (HQ Graphene). The bare-WSe₂/MoS₂ monolayer samples were directly exfoliated at 105 °C from bulk crystals on SiO₂/Si substrates pretreated by oxygen plasma. The PDMS-WSe₂/MoS₂ monolayer samples were exfoliated to a PDMS stamp (PF Film X4 from Gel-Pak) and transferred to the SiO₂/Si substrates pretreated by oxygen plasma. The van der Waals heterostructure samples were fabricated by a PMMA-assisted dry-transfer technique. The details can be found in Figure S1.

Simulations. The dielectric screening properties of the graphene-boron nitride heterostructure was calculated based on density functional theory (DFT) and many-body perturbation theory using norm-conserving pseudopotentials and local density approximations (LDA) for the exchange-correlation functional, ^{60,61} as implemented in the Quantum Espresso package. A supercell consists of a graphene layer and two layers of boron nitride was constructed to evaluate the fluctuation of the periodic dielectric constants in a moiré pattern. The dielectric matrix of the heterostructure was calculated using the BerkeleyGW code. The computational details are listed in the Supporting Information document.

Optical Measurements. All low-temperature measurements were performed in a He-flow cryostat (AttoDRY800). The samples were optically pumped using a 3.06 eV picosecond laser diode (PDL 800-D, 30 ps pulse width) focused to the diffraction limit spot for PL measurements. The PL signal was directed to a spectrometer (IsoPlane-320 from Princeton Instruments), dispersed by a diffraction grating (300 grooves per mm) and detected by a CCD camera (PIXIS: 400BR). A halogen lamp is used as a white light source for the optical reflection contrast spectroscopy. The white light signal was directed to a spectrometer (HRS-300 from Princeton Instruments), dispersed by a diffraction grating (300 grooves per mm) and detected by a CCD camera (PIXIS: 1024). The reflection contrast $(\Delta R/R)$ spectrum is obtained by comparing the reflected white light spectrum from the sample (R_0) with that from the substrate next to the sample (R) as $\Delta R/R = (R_0)$ R)/R. Time-resolved photoluminescence and spatially resolved imaging of the interlayer exciton emission was achieved using a time-correlated single-photon counting module (HydraHarp 400) and a single-photon avalanche photodiode (Micro Photon Devices). A picosecond laser diode head (PDL 800-D, 30 ps pulse width) at 3.06 eV was used to excite the samples. A 405 nm dichroic filter set was used in the excitation path.

ASSOCIATED CONTENT

Supporting Information

The Supporting Information is available free of charge at https://pubs.acs.org/doi/10.1021/acs.nanolett.1c02990.

Sample fabrication, AFM scans, WSe₂ PL spectrum at 4.2 K, effect of dielectric disorders on defect states, Auger recombination, Auger broadening, multi-trapping (MT) exciton transport with an exponential distribution of trap states, first-principles calculations, moiré replica, periodic dielectric disorder from the h-BN/Gr moiré

superlattice on another sample, and halo effect at 18.2 μ J/cm² laser fluence (PDF)

AUTHOR INFORMATION

Corresponding Author

Parag B. Deotare — Electrical and Computer Engineering Department and Applied Physics Program, University of Michigan, Ann Arbor, Michigan 48109, United States; orcid.org/0000-0002-9867-7380; Email: pdeotare@umich.edu

Authors

- Zidong Li Electrical and Computer Engineering Department, University of Michigan, Ann Arbor, Michigan 48109, United States; orcid.org/0000-0002-0984-9778
- Darwin F. Cordovilla Leon Electrical and Computer Engineering Department and Applied Physics Program, University of Michigan, Ann Arbor, Michigan 48109, United States
- Woncheol Lee Electrical and Computer Engineering Department, University of Michigan, Ann Arbor, Michigan 48109, United States
- Kanak Datta Electrical and Computer Engineering
 Department, University of Michigan, Ann Arbor, Michigan
 48109, United States; © orcid.org/0000-0003-4086-3225
- Zhengyang Lyu Applied Physics Program, University of Michigan, Ann Arbor, Michigan 48109, United States
- Jize Hou Electrical and Computer Engineering Department, University of Michigan, Ann Arbor, Michigan 48109, United States
- Takashi Taniguchi International Center for Materials Nanoarchitectonics, National Institute for Materials Science, Tsukuba 305-0044, Japan; ⊚ orcid.org/0000-0002-1467-3105
- Kenji Watanabe Research Center for Functional Materials, National Institute for Materials Science, Tsukuba 305-0044, Japan; © orcid.org/0000-0003-3701-8119
- Emmanouil Kioupakis Department of Materials Science and Engineering, University of Michigan, Ann Arbor, Michigan 48109, United States; orcid.org/0000-0003-1880-6443

Complete contact information is available at: https://pubs.acs.org/10.1021/acs.nanolett.1c02990

Author Contributions

P.D. and Z. Li conceived the idea. P.D. supervised the project. Z.Li and J.H. fabricated the devices. Z. Li performed the optical measurements. Z. Li and Z. Lyu analyzed the data. D.C.L. contributed to multitrapping and release model. W.L. performed the first-principles calculations supervised by E.K. K.D. performed the AFM measurement. K.W. and T.T. provided the bulk h-BN crystals. All authors contributed to the writing of the manuscript. The authors also thank Dr. M. Florian and Prof. M. Kira for valuable discussions.

Notes

The authors declare no competing financial interest.

ACKNOWLEDGMENTS

This work was supported through the National Science Foundation (NSF) grant No. DMR-1904541. D.C.L. acknowledges support from the University of Michigan's Rackham Merit Fellowship and the NSF Graduate Research Fellowship

Program under Grant No. DGE 1256260. W.L. was partially supported by the Kwanjeong Educational Foundation Scholarship. Computational resources were provided by the National Energy Research Scientific Computing (NERSC) Center, a DOE office of Science User Facility supported under Contract No. DE-AC02- 05CH11231. K.W. and T.T. acknowledge support from the Elemental Strategy Initiative conducted by the MEXT, Japan (grant no. JPMXP0112101001) and JSPSKAKENHI (grant nos. JP19H05790 and JP20H00354).

REFERENCES

- (1) Van Tuan, D.; Yang, M.; Dery, H. Coulomb Interaction in Monolayer Transition-Metal Dichalcogenides. *Phys. Rev. B: Condens. Matter Mater. Phys.* **2018**, 98 (12), 1–13.
- (2) Wang, D.; Sundararaman, R. Substrate Effects on Charged Defects in Two-Dimensional Materials. *Phys. Rev. Mater.* **2019**, 3 (8), 1–8.
- (3) Raja, A.; Waldecker, L.; Zipfel, J.; Cho, Y.; Brem, S.; Ziegler, J. D.; Kulig, M.; Taniguchi, T.; Watanabe, K.; Malic, E.; Heinz, T. F.; Berkelbach, T. C.; Chernikov, A. Dielectric Disorder in Two-Dimensional Materials. *Nat. Nanotechnol.* **2019**, *14* (9), 832–837.
- (4) Fu, Y.; He, D.; He, J.; Bian, A.; Zhang, L.; Liu, S.; Wang, Y.; Zhao, H. Effect of Dielectric Environment on Excitonic Dynamics in Monolayer WS2. *Adv. Mater. Interfaces* **2019**, *6* (23), 1901307.
- (5) Hoshi, Y.; Kuroda, T.; Okada, M.; Moriya, R.; Masubuchi, S.; Watanabe, K.; Taniguchi, T.; Kitaura, R.; Machida, T. Suppression of Exciton-Exciton Annihilation in Tungsten Disulfide Monolayers Encapsulated by Hexagonal Boron Nitrides. *Phys. Rev. B: Condens. Matter Mater. Phys.* **2017**, 95 (24), 1–6.
- (6) Newaz, A. K. M.; Puzyrev, Y. S.; Wang, B.; Pantelides, S. T.; Bolotin, K. I. Probing Charge Scattering Mechanisms in Suspended Graphene by Varying Its Dielectric Environment. *Nat. Commun.* **2012**, *3*, 734.
- (7) Lin, Y.; Ling, X.; Yu, L.; Huang, S.; Hsu, A. L.; Lee, Y. H.; Kong, J.; Dresselhaus, M. S.; Palacios, T. Dielectric Screening of Excitons and Trions in Single-Layer MoS2. *Nano Lett.* **2014**, *14* (10), 5569–5576
- (8) Nie, Z.; Shi, Y.; Qin, S.; Wang, Y.; Jiang, H.; Zheng, Q.; Cui, Y.; Meng, Y.; Song, F.; Wang, X.; Turcu, I. C. E.; Wang, X.; Xu, Y.; Shi, Y.; Zhao, J.; Zhang, R.; Wang, F. Tailoring Exciton Dynamics of Monolayer Transition Metal Dichalcogenides by Interfacial Electron-Phonon Coupling. *Commun. Phys.* **2019**, *2* (1), 1–8.
- (9) Komsa, H. P.; Kotakoski, J.; Kurasch, S.; Lehtinen, O.; Kaiser, U.; Krasheninnikov, A. V. Two-Dimensional Transition Metal Dichalcogenides under Electron Irradiation: Defect Production and Doping. *Phys. Rev. Lett.* **2012**, *109* (3), 1–5.
- (10) Qiu, H.; Xu, T.; Wang, Z.; Ren, W.; Nan, H.; Ni, Z.; Chen, Q.; Yuan, S.; Miao, F.; Song, F.; Long, G.; Shi, Y.; Sun, L.; Wang, J.; Wang, X. Hopping Transport through Defect-Induced Localized States in Molybdenum Disulphide. *Nat. Commun.* **2013**, *4*, 3–8.
- (11) Yu, Z.; Pan, Y.; Shen, Y.; Wang, Z.; Ong, Z. Y.; Xu, T.; Xin, R.; Pan, L.; Wang, B.; Sun, L.; Wang, J.; Zhang, G.; Zhang, Y. W.; Shi, Y.; Wang, X. Towards Intrinsic Charge Transport in Monolayer Molybdenum Disulfide by Defect and Interface Engineering. *Nat. Commun.* **2014**, *5*, 1–7.
- (12) Perea-Causín, R.; Brem, S.; Rosati, R.; Jago, R.; Kulig, M.; Ziegler, J. D.; Zipfel, J.; Chernikov, A.; Malic, E. Exciton Propagation and Halo Formation in Two-Dimensional Materials. *Nano Lett.* **2019**, 19 (10), 7317–7323.
- (13) Glazov, M. M. Phonon Wind and Drag of Excitons in Monolayer Semiconductors. *Phys. Rev. B: Condens. Matter Mater. Phys.* **2019**, *100* (4), 45426.
- (14) Kulig, M.; Zipfel, J.; Nagler, P.; Blanter, S.; Schüller, C.; Korn, T.; Paradiso, N.; Glazov, M. M.; Chernikov, A. Exciton Diffusion and Halo Effects in Monolayer Semiconductors. *Phys. Rev. Lett.* **2018**, *120* (20), 207401.
- (15) Zipfel, J.; Kulig, M.; Perea-Causin, R.; Brem, S.; Ziegler, J. D.; Rosati, R.; Taniguchi, T.; Watanabe, K.; Glazov, M. M.; Malic, E.;

- Chernikov, A. Exciton diffusion in monolayer semiconductors with suppressed disorder. *Phys. Rev. B: Condens. Matter Mater. Phys.* **2020**, 101. 115430.
- (16) Zipfel, J.; Kulig, M.; Perea-Causín, R.; Brem, S.; Ziegler, J. D.; Rosati, R.; Taniguchi, T.; Watanabe, K.; Glazov, M. M.; Malic, E.; Chernikov, A. Exciton Diffusion in Monolayer Semiconductors with Suppressed Disorder. *Phys. Rev. B: Condens. Matter Mater. Phys.* **2020**, 101, 115430.
- (17) Yu, Y.; Bataller, A. W.; Younts, R.; Yu, Y.; Li, G.; Puretzky, A. A.; Geohegan, D. B.; Gundogdu, K.; Cao, L. Roomerature Electron-Hole Liquid in Monolayer MoS2. *ACS Nano* **2019**, *13* (9), 10351–10358.
- (18) Arp, T. B.; Pleskot, D.; Aji, V.; Gabor, N. M. Electron-Hole Liquid in a van Der Waals Heterostructure Photocell at Room Temperature. *Nat. Photonics* **2019**, *13* (4), 245–250.
- (19) Castellanos-Gomez, A.; Buscema, M.; Molenaar, R.; Singh, V.; Janssen, L.; Van Der Zant, H. S. J.; Steele, G. A. Deterministic Transfer of Two-Dimensional Materials by All-Dry Viscoelastic Stamping. 2D Mater. **2014**, *1* (1), 011002.
- (20) Stier, A. V.; Wilson, N. P.; Clark, G.; Xu, X.; Crooker, S. A. Probing the Influence of Dielectric Environment on Excitons in Monolayer WSe2: Insight from High Magnetic Fields. *Nano Lett.* **2016**, *16* (11), 7054–7060.
- (21) Li, Z.; Wang, T.; Lu, Z.; Jin, C.; Chen, Y.; Meng, Y.; Lian, Z.; Taniguchi, T.; Watanabe, K.; Zhang, S.; Smirnov, D.; Shi, S. F. Revealing the Biexciton and Trion-Exciton Complexes in BN Encapsulated WSe2. *Nat. Commun.* **2018**, *9* (1), 1–7.
- (22) Ye, Z.; Waldecker, L.; Ma, E. Y.; Rhodes, D.; Antony, A.; Kim, B.; Zhang, X. X.; Deng, M.; Jiang, Y.; Lu, Z.; Smirnov, D.; Watanabe, K.; Taniguchi, T.; Hone, J.; Heinz, T. F. Efficient Generation of Neutral and Charged Biexcitons in Encapsulated WSe2Monolayers. *Nat. Commun.* **2018**, *9* (1), 6–11.
- (23) Chen, S. Y.; Goldstein, T.; Taniguchi, T.; Watanabe, K.; Yan, J. Coulomb-Bound Four- and Five-Particle Intervalley States in an Atomically-Thin Semiconductor. *Nat. Commun.* **2018**, *9* (1), 1–8.
- (24) Li, Z.; Wang, T.; Jin, C.; Lu, Z.; Lian, Z.; Meng, Y.; Blei, M.; Gao, M.; Taniguchi, T.; Watanabe, K.; Ren, T.; Cao, T.; Tongay, S.; Smirnov, D.; Zhang, L.; Shi, S. F. Momentum-Dark Intervalley Exciton in Monolayer Tungsten Diselenide Brightened via Chiral Phonon. ACS Nano 2019, 13 (12), 14107–14113.
- (25) Li, Z.; Wang, T.; Jin, C.; Lu, Z.; Lian, Z.; Meng, Y.; Blei, M.; Gao, S.; Taniguchi, T.; Watanabe, K.; Ren, T.; Tongay, S.; Yang, L.; Smirnov, D.; Cao, T.; Shi, S. F. Emerging Photoluminescence from the Dark-Exciton Phonon Replica in Monolayer WSe2. *Nat. Commun.* **2019**, *10* (1), 1–7.
- (26) Li, Z.; Wang, T.; Lu, Z.; Khatoniar, M.; Lian, Z.; Meng, Y.; Blei, M.; Taniguchi, T.; Watanabe, K.; McGill, S. A.; Tongay, S.; Menon, V. M.; Smirnov, D.; Shi, S. F. Direct Observation of Gate-Tunable Dark Trions in Monolayer WSe2. *Nano Lett.* **2019**, *19* (10), 6886–6893
- (27) He, M.; Rivera, P.; Van Tuan, D.; Wilson, N. P.; Yang, M.; Taniguchi, T.; Watanabe, K.; Yan, J.; Mandrus, D. G.; Yu, H.; Dery, H.; Yao, W.; Xu, X. Valley Phonons and Exciton Complexes in a Monolayer Semiconductor. *Nat. Commun.* **2020**, *11* (1), 1–7.
- (28) Cordovilla Leon, D. F.; Li, Z.; Jang, S. W.; Deotare, P. B. Hot Exciton Transport in WSe₂ Monolayers. *Phys. Rev. B: Condens. Matter Mater. Phys.* **2019**, 100 (24), 241401.
- (29) Wang, G.; Chernikov, A.; Glazov, M. M.; Heinz, T. F.; Marie, X.; Amand, T.; Urbaszek, B. Colloquium: Excitons in Atomically Thin Transition Metal Dichalcogenides. *Rev. Mod. Phys.* **2018**, 90 (2), No. 021001.
- (30) Latini, S.; Olsen, T.; Thygesen, K. S. Excitons in van Der Waals Heterostructures: The Important Role of Dielectric Screening. *Phys. Rev. B: Condens. Matter Mater. Phys.* **2015**, 92 (24), 1–13.
- (31) Andersen, K.; Latini, S.; Thygesen, K. S. Dielectric Genome of van Der Waals Heterostructures. *Nano Lett.* **2015**, *15* (7), 4616–4621.
- (32) Mitterreiter, E.; Schuler, B.; Micevic, A.; Hernangómez-Pérez, D.; Barthelmi, K.; Cochrane, K. A.; Kiemle, J.; Sigger, F.; Klein, J.;

- Wong, E.; Barnard, E. S.; Watanabe, K.; Taniguchi, T.; Lorke, M.; Jahnke, F.; Finley, J. J.; Schwartzberg, A. M.; Qiu, D. Y.; Refaely-Abramson, S.; Holleitner, A. W.; Weber-Bargioni, A.; Kastl, C. The Role of Chalcogen Vacancies for Atomic Defect Emission in MoS2. *Nat. Commun.* **2021**, *12* (1), 1–8.
- (33) Venanzi, T.; Arora, H.; Erbe, A.; Pashkin, A.; Winnerl, S.; Helm, M.; Schneider, H. Exciton Localization in MoSe2Monolayers Induced by Adsorbed Gas Molecules. *Appl. Phys. Lett.* **2019**, *114* (17), 172106
- (34) Li, H.; Huang, M.; Cao, G. Markedly Different Adsorption Behaviors of Gas Molecules on Defective Monolayer MoS2: A First-Principles Study. *Phys. Chem. Chem. Phys.* **2016**, *18* (22), 15110–15117.
- (35) Moody, G.; Tran, K.; Lu, X.; Autry, T.; Fraser, J. M.; Mirin, R. P.; Yang, L.; Li, X.; Silverman, K. L. Microsecond Valley Lifetime of Defect-Bound Excitons in Monolayer WSe2. *Phys. Rev. Lett.* **2018**, *121* (5), 57403.
- (36) Rivera, P.; He, M.; Kim, B.; Liu, S.; Rubio-Verdú, C.; Moon, H.; Mennel, L.; Rhodes, D. A.; Yu, H.; Taniguchi, T. Intrinsic Donor-Bound Excitons in Ultraclean Monolayer Semiconductors. *Nat. Commun.* **2021**, *12*, 871.
- (37) Paur, M.; Molina-Mendoza, A. J.; Bratschitsch, R.; Watanabe, K.; Taniguchi, T.; Mueller, T. Electroluminescence from Multi-Particle Exciton Complexes in Transition Metal Dichalcogenide Semiconductors. *Nat. Commun.* **2019**, *10* (1), 1–7.
- (38) Chow, P. K.; Jacobs-Gedrim, R. B.; Gao, J.; Lu, T. M.; Yu, B.; Terrones, H.; Koratkar, N. Defect-Induced Photoluminescence in Monolayer Semiconducting Transition Metal Dichalcogenides. *ACS Nano* **2015**, *9* (2), 1520–1527.
- (39) Cadiz, F.; Courtade, E.; Robert, C.; Wang, G.; Shen, Y.; Cai, H.; Taniguchi, T.; Watanabe, K.; Carrere, H.; Lagarde, D.; Manca, M.; Amand, T.; Renucci, P.; Tongay, S.; Marie, X.; Urbaszek, B. Excitonic Linewidth Approaching the Homogeneous Limit in MoS2-Based van Der Waals Heterostructures. *Phys. Rev. X* **2017**, *7* (2), No. 021026.
- (40) Greben, K.; Arora, S.; Harats, M. G.; Bolotin, K. I. Intrinsic and Extrinsic Defect-Related Excitons in TMDCs. *Nano Lett.* **2020**, *20* (4), 2544–2550.
- (41) Huang, X.; Li, Z.; Liu, X.; Hou, J.; Kim, J.; Forrest, S. R.; Deotare, P. B. Neutralizing Defect States in MoS2Monolayers. ACS Appl. Mater. Interfaces 2021, 13 (37), 44686–44692.
- (42) Noh, J. Y.; Kim, H.; Park, M.; Kim, Y. S. Deep-to-Shallow Level Transition of Re and Nb Dopants in Monolayer MoS2 with Dielectric Environments. *Phys. Rev. B: Condens. Matter Mater. Phys.* **2015**, 92 (11), 6–9.
- (43) Akselrod, G. M.; Deotare, P. B.; Thompson, N. J.; Lee, J.; Tisdale, W. A.; Baldo, M. A.; Menon, V. M.; Bulovic, V. Visualization of Exciton Transport in Ordered and Disordered Molecular Solids. *Nat. Commun.* **2014**, *5*, 1–8.
- (44) Cordovilla Leon, D. F.; Li, Z.; Jang, S. W.; Cheng, C.-H.; Deotare, P. B. Exciton Transport in Strained Monolayer WSe2. *Appl. Phys. Lett.* **2018**, *113* (25), 252101.
- (45) Mady, F.; Reboul, J. M.; Renoud, R. Formal Analogy between Multiple-Trapping and Polarization Models: A Physical Picture for the Cole-Cole Formula. *J. Phys. D: Appl. Phys.* **2005**, 38 (13), 2271–2275.
- (46) Hughes, A. E.; Pells, G. P. The Luminescence Spectra of Bi3+ Ions in MgO and CaO. *Phys. Status Solidi B* 1975, 71 (2), 707–718. (47) Liu, X.; Yu, H.; Ji, Q.; Gao, Z.; Ge, S.; Qiu, J.; Liu, Z.; Zhang, Y.; Sun, D. An Ultrafast Terahertz Probe of the Transient Evolution of the Charged and Neutral Phase of Photo-Excited Electron-Hole Gas
- in a Monolayer Semiconductor. 2D Mater. 2016, 3 (1), 014001. (48) Li, Z.; Lu, X.; Cordovilla Leon, D. F.; Lyu, Z.; Xie, H.; Hou, J.; Lu, Y.; Guo, X.; Kaczmarek, A.; Taniguchi, T.; Watanabe, K.; Zhao, L.; Yang, L.; Deotare, P. B. Interlayer Exciton Transport in MoSe₂/WSe₂ Heterostructures. ACS Nano 2021, 15 (1), 1539–1547.
- (49) Gao, T.; Song, X.; Du, H.; Nie, Y.; Chen, Y.; Ji, Q.; Sun, J.; Yang, Y.; Zhang, Y.; Liu, Z. Temperature-Triggered Chemical

- Switching Growth of in-Plane and Vertically Stacked Graphene-Boron Nitride Heterostructures. *Nat. Commun.* **2015**, *6*, 6835.
- (50) Giovannetti, G.; Khomyakov, P. A.; Brocks, G.; Kelly, P. J.; Van Den Brink, J. Substrate-Induced Band Gap in Graphene on Hexagonal Boron Nitride: Ab Initio Density Functional Calculations. *Phys. Rev. B: Condens. Matter Mater. Phys.* **2007**, *76* (7), 2–5.
- (51) Moon, P.; Koshino, M. Electronic Properties of Graphene/Hexagonal-Boron-Nitride Moiré Superlattice. *Phys. Rev. B: Condens. Matter Mater. Phys.* **2014**, 90 (15), 1–12.
- (52) Xu, Y.; Horn, C.; Zhu, J.; Tang, Y.; Ma, L.; Li, L.; Liu, S.; Watanabe, K.; Taniguchi, T.; Hone, J. C.; Shan, J.; Mak, K. F. Creation of Moiré Bands in a Monolayer Semiconductor by Spatially Periodic Dielectric Screening. *Nat. Mater.* **2021**, *20*, 645–649.
- (53) Goodman, A. J.; Lien, D. H.; Ahn, G. H.; Spiegel, L. L.; Amani, M.; Willard, A. P.; Javey, A.; Tisdale, W. A. Substrate-Dependent Exciton Diffusion and Annihilation in Chemically Treated MoS2and WS2. J. Phys. Chem. C 2020, 124 (22), 12175–12184.
- (54) Steinhoff, A.; Florian, M.; Jahnke, F. Microscopic Theory of Exciton-Exciton Annihilation in Two-Dimensional Semiconductors. arXiv (Mesoscale and Nanoscale Physics), June 30, 2021, arXiv:2106.15973, ver. 2. https://arxiv.org/pdf/2106.15973.pdf (accessed June 30, 2021).
- (55) Hänggi, P.; Talkner, P.; Borkovec, M. Reaction-Rate Theory: Fifty Years after Kramers. Rev. Mod. Phys. 1990, 62 (2), 251–341.
- (56) Ala-Nissila, T.; Ferrando, R.; Ying, S. C. Collective and Single Particle Diffusion on Surfaces. *Adv. Phys.* **2002**, *51* (3), 949–1078.
- (57) Datta, K.; Lyu, Z.; Li, Z.; Taniguchi, T.; Watanabe, K.; Deotare, P. B. Spatiotemporally Controlled Room Temperature Exciton Transport under Dynamic Pressure. *arxiv* (Mesoscale and Nanoscale Physics), Aug. 13, 2021, arXiv:2108.06418.https://arxiv.org/ftp/arxiv/papers/2108/2108.06418.pdf (accessed Aug. 13, 2021).
- (58) Grosso, G.; Graves, J.; Hammack, A. T.; High, A. A.; Butov, L. V.; Hanson, M.; Gossard, A. C. Excitonic Switches Operating at around 100K. *Nat. Photonics* **2009**, *3* (10), 577–580.
- (59) Unuchek, D.; Ciarrocchi, A.; Avsar, A.; Watanabe, K.; Taniguchi, T.; Kis, A. Room-Temperature Electrical Control of Exciton Flux in a van Der Waals Heterostructure. *Nature* **2018**, *560* (7718), 340–344.
- (60) Ceperley, D. M.; Alder, B. J. Ground State of the Electron Gas by a Stochastic Method. *Phys. Rev. Lett.* **1980**, *45* (7), 566–569.
- (61) Perdew, J. P.; Zunger, A. Self-Interaction Correction to Density-Functional Approximations for Many-Electron Systems. *Phys. Rev. B: Condens. Matter Mater. Phys.* **1981**, 23 (10), 5048–5079.
- (62) Giannozzi, P.; Baroni, S.; Bonini, N.; Calandra, M.; Car, R.; Cavazzoni, C.; Ceresoli, D.; Chiarotti, G. L.; Cococcioni, M.; Dabo, I. QUANTUM ESPRESSO: A Modular and Open-Source Software Project for Quantum Simulations of Materials. *J. Phys.: Condens. Matter* 2009, 21 (39), 395502.
- (63) Deslippe, J.; Samsonidze, G.; Strubbe, D. A.; Jain, M.; Cohen, M. L.; Louie, S. G. BerkeleyGW: A Massively Parallel Computer Package for the Calculation of the Quasiparticle and Optical Properties of Materials and Nanostructures. *Comput. Phys. Commun.* **2012**, *183* (6), 1269–1289.